Surfaces and Interfaces 44 (2024) 103627

Contents lists available at ScienceDirect

Surfaces and Interfaces

journal homepage: www.sciencedirect.com/journal/surfaces-and-interfaces

Suppression of back electron recombination on the photoanode-electrolyte interface with poly(4-vinylbenzoic acid) and poly(4-vinylpyridine) co-adsorbents for stable and efficient dye-sensitized solar cells

Daniela F.S.L. Rodrigues [a,c], Jorge Martins [c,d], Frédéric SAUVAGE [e], Carlos M.R. Abreu [a], Jorge F.J. Coelho [a,b], Arménio C. Serra [a,*], Dzmitry Ivanou [c,d,*], Adélio Mendes [c,d]

[a] University of Coimbra, CEMMPRE, ARISE, Department of Chemical Engineering, Rua Sílvio Lima – Polo II, 3030-790 Coimbra, Portugal
[b] IPN, Instituto Pedro Nunes, Associação para a Inovação e Desenvolvimento em Ciência e Tecnologia, Rua Pedro Nunes, 3030-199 Coimbra, Portugal
[c] LEPABE, Departamento de Engenharia Química, Faculdade de Engenharia, Universidade do Porto, Rua Dr. Roberto Frias, 4200-465 Porto, Portugal
[d] ALiCE - Associate Laboratory in Chemical Engineering, Faculty of Engineering, University of Porto, Rua Dr. Roberto Frias, Porto 4200-465, Portugal
[e] Laboratoire de Réactivité et Chimie des Solides, Université de Picardie Jules Verne (UPJV), CNRS UMR 7314, Hub de l'énergie, 15 rue Baudelocque, 80039 Amiens, France

ARTICLE INFO

Keywords:
Dye-sensitized solar cells
Co-adsorbents
Polymers
Back electron recombination
Photoanode-electrolyte interface

ABSTRACT

Dye-sensitized solar cells (DSSC) are one of the most intensively developing PV technology to meet the emerging needs of wireless power for billions of IoT devices and wireless electronics; DSSCs have recently entered the indoor PV market. Suppressors of back electron recombination on the photoanode-electrolyte interface, also known as co-adsorbents, are key components of the DSSCs to obtain high power conversion efficiencies (PCE). Chenodeoxycholic acid (CDCA), yet obtained by extraction from the animal liver, dominates among other co-adsorbent and enables devices with the highest PCE and long lifetime. Achieving adequate PCE with long-term device stability with CDCA alternatives is a challenge addressed in this study using poly4-vinylbenzoic acid (PVBA) and poly(4-vinylpyridine) (P4VP). Polymeric co-adsorbents effectively suppress electron transfer from the TiO_2/N719 photoanode to $I_3^-/3I^-$ electrolyte resulting in decently performing devices with 1-sun equivalent PCEs of 8.3 % and 9 %, respectively; 17.5 % and 22 % of artificial light PCEs were achieved. The presence of the polymer hampers molecular dye aggregation within the self-assembled monolayer; the acceleration of the charge injection and excited dye prolonging was monitored by Time-Correlated Single Photon Counting photoluminescence spectroscopy. Intrinsic device degradation in the accelerated light soaking test was assessed according to ISOS-L2 protocol. Carboxylic-functioned molecular chain of PVBA allows stronger adsorption on the photoanode-electrolyte interface and renderes stable devices with 1000 h of PCE history equivalent to conventional CDCA.

1. Introduction

Photovoltaic (PV) devices based on dye-sensitized solar cells (DSSC) have attracted tremendous research interest during the past thirty years, due to the cheap fabrication process, ability to be incorporated in flexible and semi-transparent modules with aesthetic appearance, sustainability, and good photocurrent conversion efficiency (PCE) to name just a few features of this technology [1–3]. The record 13 % PCE under simulated 1-Sun illumination has been certified [4], and a new breakthrough with an independently confirmed 15.2 % PCE was recently unveiled [5].

Building- and agriculture-integrated PV installations traditionally consider DSSCs amongst desirable assets [6,7]. Emerging DSSCs developments and research trends, to name a few, include aqueous [8] and bio-source derived [9] devices, integration of DSSCs in energy storage systems [10], solar-rechargeable redox flow batteries [11,12], water-splitting applications [13], and wearable electronics [14–16]. The current demand for wireless power from the internet of things (IoT) and low-power-consuming electronics has made DSSCs one of the most efficient and rapidly developing indoor PV systems [17–19]. Amazing PCE values of about 30–35 % [4,20,21] has been reported under artificial indoor light, and PCE values of *ca.* 40 % are considered realistically

* Corresponding authors.
E-mail addresses: rmenio.serra@gmail.com (A.C. Serra), ivanou@fe.up.pt (D. Ivanou).

https://doi.org/10.1016/j.surfin.2023.103627
Received 3 May 2023; Received in revised form 28 October 2023; Accepted 11 November 2023
Available online 13 November 2023

feasible for this technology [22]. Following, several companies have recently begun to enter the market with indoor DSSCs [1,23]. The development of new materials that are attractive in terms of price, simplicity, abundance, device efficiency, and stability is critical to the market success of DSSCs.

The suppressors of back-electron transfer on photoanode-electrolyte interface and dye desegregation additives are one of the most critical integral components of an efficient DSSC device [5,24-28]. Recombination suppressors intentionally co-adsorbed on the mesoporous scaffold along with the sensitizer, by adding them to the dye solution during the sensitization step, allowing them to adsorb after the dye loading, or adding to the electrolyte [26]. In classical understanding, co-adsorbents suppress electron transfer from the dye framework layer to the electrolyte, affect the position and distribution of localized intraband gap states due to the dipole modification, and prevent dye aggregation; make the photocurrent density and open circuit potential to increase, which has a positive effect on the overall PCE [26–28]. Emerging research in developing co-adsorbents involves strategies to combine the capabilities of dye desegregation and surface passivation while incorporating advantageous functions like co-sensitization [29] or hole transport [30,31]; the efforts aim to enhance the efficiency of photocurrent yield and dye regeneration.

The benchmark co-adsorbent used for best-performing and long-term stable DSSCs is the chenodeoxycholic acid (CDCA). As one of the primary bile acids, CDCA was first described in 1993 as a recombination suppressor and dye desegregation additive for DSSCs [32]. CDCA efficiently passivates the TiO_2 surface, hinders reverse current, promotes dye dispersion, and increases the TiO_2 Fermi level position, thereby enhancing charge separation [33–37]. However, CDCA is a relatively expensive co-adsorbent. It has a complex structure that makes direct chemical synthesis difficult; extraction from animal liver [38] is a dominant approach for commercial production of this unique co-adsorbent.

Tremendous efforts have been made to search for CDCA alternatives in simpler compounds: carboxylic and phosphoric esters of acids, diphenylic or dineohexyl phosphinic acids, decylphosphonic acid, amines, 4-tertbutylpyridine to name a few; unfortunately, either PCE or long-term device stability was sacrificed by replacing CDCA [26]. Promising recombination suppressing behavior in N719-sensitized photoanodes was shown by long-chain molecules, i.e. the polymers, due to improved sorption and surface coverage abilities; however, all reported to date result in devices that underperform [39–42] when compared with devices employing CDCA, which easily achieve a PCE of *ca.* 9 % [43,44]. Coordinately adsorbed poly(ethylene glycol) on TiO_2 shifts the conduction band edge of titanium dioxide downward and suppresses titania dark current, leading to an improvement in PCE from 4.6 % in a pristine reference to 5.6 % [39]. Polystyrene with terminal carboxylic-acid groups leads to an increase in electron lifetime and 5.7 % of PCE [40]. Polymerised on photoanode of tetraethyl orthosilicate [41] or methylmethacrylate/1,6-hexandiol diacrylate [42] allowed an overall PCE of 5.6 % and 7.8 %, respectively.

Previous findings suggest that sorption and recombination suppression efficacy of co-adsorbents are determined by the chemistry of the anchoring groups and the molecular structure, which is important to consider when developing efficient co-adsorbents for durable devices. The authors have recently reported that poly(4-vinylpyridine) (P4VP) coordinately bonded to titanium dioxide via nitrogen heteroatom and acts as a very efficient suppressor of electron recombination when the molecular weight and co-adsorption conditions are properly adjusted; in addition, P4VP promotes dye anchoring which favors electron extraction from the photoexcited dye [45]. Photoanodes passivated with P4VP, enable a PCE of over 9 % and 22 % under 1-Sun equivalent and artificial 1000 lx light, respectively. The photovoltaic performance of the devices fabricated with cheap fully synthetic P4VP co-adsorbed is competitive with conventional CDCA-passivated counterparts, which was very promising, considering the absolute stability of 300 h under aging in the dark (ISOS-D-1 testing conditions [46]). Unfortunately, the disadvantage of P4VP co-adsorbent has been demonstrated when applying different stability certification protocols, as shown in this article. A rapid drop in PCE was observed in the accelerated light soaking test; the sorption strength of P4VP on the photoanode is insufficient to ensure long device lifespan.

Encouraged by the good primary PCE with the new co-adsorbent P4VP, this work describes moleculary improved homopolymer similar to P4VP chain and length but intentionally endowed with carboxylic anchoring groups to achieve stronger bonding to TiO_2 surface - poly-4-vinylbenzoic acid (PVBA). P4VP and PVBA were comparatively investigated as co-adsorbing additives in DSSCs to determine the effects of anchoring group chemistry on polymer sorption, dye interaction, photocurrent generation, back electron recombination suppression, device photovoltaic performance, and long-term stability; the relevance of the "proper" chemical design of anchoring groups in new polymeric co-adsorbent on device stability and overall PCE is emphasized.

For the first time, the polymeric co-adsorbent PVBA provided devices with PCE of 8.3 % and 17.5 % under 1-Sun and artificial 1000 lx light, respectively, with the same stability as with CDCA, under accelerated aging in light soaking according. This makes PVBA an attractive synthetic recombination suppressor for efficient yet, highly stable devices; relevant to commercial DSSCs production.

2. Experimental section

2.1. Preparation of poly(4-vinylbenzoic acid) and poly(4-vinylpyridine) homopolymers

Poly(4-vinylbenzoic acid) (PVBA) homopolymer with MW of 10.3 kg mol^{-1} was synthesized by RAFT polymerization [47,48] as described in Supporting Information. ^{1}H-NMR spectroscopy (**Fig. S1**) confirmed the structure of the obtained product. PVBA was obtained with a low dispersity ($Đ$) (< 1.2) (**Table S1**); the molecular weight (MW) distribution curve of PVBA was obtained by size exclusion chromatography (SEC) (**Fig. S2**). Poly(4-vinylpyridine) (P4VP) homopolymer with MW of 8.5 kg mol^{-1} was prepared as described in our previous study [45].

2.2. Fabrication of DSSCs

The procedure of DSSCs assembling follows the protocol described in detail elsewhere [43,44]. Briefly, FTO-coated glasses (TEC-7; GreatCell Solar) served as substrates for photoanode and counter electrode.

A dense layer of TiO_2 (80 ± 5 nm thick) was deposited on FTO glasses used for photoanodes by spray pyrolysis at 450 °C. The solution for TiO_2 spray deposition was composed of 7.0 mL anhydrous i-PrOH, 0.6 mL titanium diisopropoxide bis(acetylacetonate) and 0.4 mL of acetylacetone, all purchased from Sigma-Aldrich. A mesoporous TiO_2 scaffold for dye adsorption was formed on the as-deposited TiO_2 blocking layer; 30NR-D and 18NR-AO TiO_2 pastes (GreatCell Solar) were sequentially screen-printed to obtain a transparent (14 μm) and active light scattering (7 μm) TiO_2 layers, respectively. A circular-shaped (0.13 cm^2) and a square-shaped (0.25 cm^2) photoanodes were formed in the devices for routine characterization (*I-V*, EIS) and assessing long-term stability under simulated light soaking, respectively. Sintering of the TiO_2 pastes was performed at 500 °C for 1 h. The photoanode substrates with a mesoporous layer of TiO_2 were treated with $TiCl_4$ aqueous solution (70 °C, 20 min), dried, and sintered at 500 °C for 1 h.

FTO glasses for counter-electrodes were drilled with two holes for electrolyte injection. FTO layer was activated with Pt nanoparticles by doctor blading of Platisol T/SP (Solaronix) paste and sintering it at 500 °C for 1 h.

The mesoporous TiO_2 layers were sensitized by sequential adsorption of N719 dye and polymer. The photoanodes were first immersed in 0.3 mM N719 dye solution in absolute ethanol for 24 h. After rinsing with ethanol, the photoanodes were transferred to an ethanolic solution

of the polymer (PVBA or P4VP) for the next 12 h [45]. After polymer adsorption, the photoanodes were rinsed with ethanol, dried in nitrogen flow, and sandwiched with a counter electrode.

The photoanodes and counter electrodes were sealed in a hot press using a 60 μm Surlyn gasket for routine short-term characterization of the devices. A high-performing commercial iodine electrolyte based on acetonitrile:valaronitrile solvent mixture (EL-HPE, GreatCell Solar) was injected into the cells; the injection holes were sealed with lamella glass and 25 μm Surlyn film.

The long-term stability of the DSSCs according to the modified ISOS-L2 protocol [46] was assessed in entirely glass-frit encapsulated cells filled with conventional 3-methoxypropionitrile-based iodine electrolyte (EL-HSE, GreatCell Solar). Encapsulation with glass frit ensures the complete tightness of the device [49–52]; however, only when the electrolyte injection holes are also glass-sealed [52]. It complies with MIL-STD-883 standard [53] for helium gas leakage; hermeticity is maintained after durability testing with humidity-freeze cycles following IEC 61646 protocol [54], as reported [52]. Robust and hermetic incapsulation is mandatory for trustworthy assessment of intrinsic degradation of the device; all extrinsic factors like oxygen and moisture ingress or electrolyte leakage must be eliminated [55]. Typical photographs of the glass-sealed devices are presented in Fig. 1.

For details on preparing fully glass-incapsulated DSSCs at process temperatures below 110 °C, including electrolyte injection holes glass sealing at room temperature [52], interested readers can consult a recently published studies [49–51].

2.3. Characterization

Current-voltage (*I-V*) characteristics of DSSCs were obtained using a Zennium (Zahner) electrochemical station at a temperature of 21 ± 1 °C. Simulated sunlight (AM1.5G, 100 mW cm^{-2}) was generated with the MiniSol solar simulator (LSH-7320, Newport); the intensity of the light flux was controlled with the calibrated Si detector. As an indoor light source, a LED lamp (Osram, Class A+, 60 W, 2700 K) with the light emission spectrum presented in **Fig. S3** was used; the LED lamp's incident light power (μW cm^{-2}) and corresponding illuminance in lux were measured with a radiometer Delta Ohm HD 2102.2. The determined light power at 500 and 1000 lx illuminance was 146 and 309 μW cm^{-2}, respectively. The PCE value of LED light was calculated as the ratio between the maximum power produced by the cells and the incident light power. For each condition, 5 similar devices were subjected to *I-V* characterization; the cells typically have a deviation interval of the PCE metrics of less than 3 %. In rare cases, devices with deviations of more than 5 % from the average of the batch were excluded from consideration.

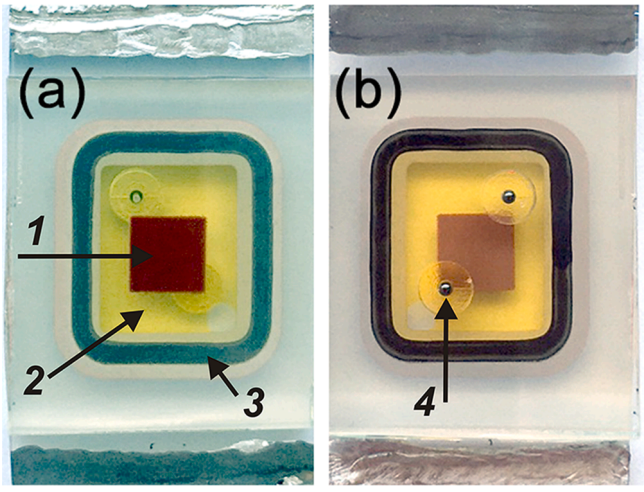

Fig. 1. Photographs of the entire glass-sealed DSSCs; photoanode (***a***) and counter electrode (***b***) sides. ***1***- photoanode; ***2*** – electrolyte; ***3*** – glass-frit sealed edge; ***4*** – glass-sealed electrolyte injection holes.

The incident photon conversion efficiency (IPCE) spectra were recorded using a setup consisting of a 300 W Xe lamp, a monochromator (Cornerstone 74125), a Lock-in amplifier with the lowest external sync frequency of 8 Hz (Merlin 70104), a set of optical filters and a light chopper. The incident photon flux was normalized with a calibrated silicon detector (Newport 70356). The bias light was supplied by a 100 W halogen lamp, and the light intensity was adjusted to 0.3 Sun-equivalent *vs.* calibrated Si-detector. The monochromatic light chopping frequency was 8.3 Hz.

Excited state lifetimes were monitored using Time-Correlated Single Photon Counting (TCSPC) technique using an Edinburgh Instrument FLS980 spectrometer. For this, we used a 80 ps pulse width laser diode as an excitation source (475 nm, 5 MHz repetition rate, ca. 4 nJ·cm^{-2} average energy. The instrument response was 90 ps FWHM measured on glass on a microchannel plate photomultiplier tube (MCP-PMT) Hamamatsu detector set after the first emission monochromator. A 515 nm long pass filter was used in emission to reject light scattering from the glass of the device. The emission was monitored at 770 nm with a slit opening of 10 nm in the emission monochromator. The numerical analysis of the excited-state lifetime has been determined after reconvolution of the photoluminescence decay considering the instrumental response function (IRF). The measurement was performed on devices without scattering layer and at open circuit condition.

Infrared spectra were obtained at room temperature using a VERTEX 70 FTIR spectrometer (BRUKER) in transmittance mode; DLaTGS detector. The spectra were collected with a resolution of 4 cm^{-1} in ATR mode, A225/Q PLATINUM ATR Diamond crystal with a single reflection accessory.

The electrochemical impedance spectroscopy (EIS) data was obtained with Autolab (PGSTAT 302 N, Metrohm). EIS spectra were recorded in the dark at a potential 20 mV below the open-circuit potential of the DSSCs; a sinusoidal perturbation of potential with a peak-to-zero amplitude of 10 mV in the frequency range of 100 kHz-1 Hz was applied. The EIS data obtained were analyzed using ZView software. The real and imaginary parts of the impedance are normalized (multiplied) to the sealing area of the device −0.36 cm^2.

A Shimadzu (UV-3600) UV-Vis-NIR spectrophotometer was used to obtain spectra of absorbance of the photoelectrodes and to quantify the amount of N719 dye adsorbed on the mesoporous TiO_2 layer. The amount of the adsorbed dye was determined using desorption of the dye in 0.5 M solution of NaOH in H_2O:EtOH (1:1, V/V). Photoanodes were immersed in 3 mL of this solution for 4 h, and the absorbance of the solution was measured. The amount of the dye was calculated using calibration data obtained by measurement of absorbance at 511 nm of the solutions with a defined concentration of the dye.

The long-term stability of the devices was assessed in a chamber (Atlas SUNTEST XLS+) equipped with AM1.5G filter, 380 nm UV-cut-off filter, and Xe-lamp as a light source. The testing protocol followed ISOS-L-2 conditions [46]; incident light intensity was 900 W m^{-2}; the temperature of the devices stabilized at 50 ± 2 °C; cells were connected to a passive load (**Fig. S4**) made from a variable resistor, which was adjusted to maintain the voltage at the maximum power point.

3. Results and discussion

3.1. Co-adsorption of PVBA and P4VP with N719 dye

Fig. 2a and b show the molecular structures of the P4VP and PVBA, respectively. Both polymer chains were intentionally designed with a small number of repeating units (*ca.* 67 and 77 for PVBA and P4VP, respectively), so that the number of groups that can potentially anchor to the TiO_2 surface is similar. The number of potential anchoring centers to titania per molecule of PVBA and P4VP far exceeds the number of

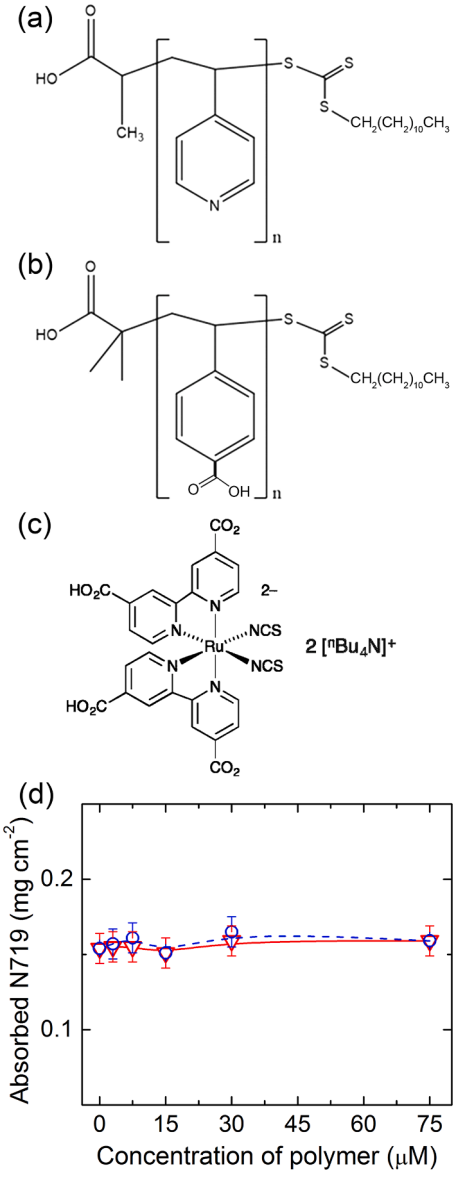

Fig. 2. Molecular structures of the P4VP (***a***), PVBA (***b***), and N719 dye (***c***). Amount of the adsorbed dye in the mesoporous titania *vs.* polymer concentration in the solution for sequential adsorption of P4VP (red triangles) and PVBA (blue circles) (***d***).

anchoring carboxylic acid groups in N719 (Fig. 2c), and sequential co-adsorption of the polymers may cause undesirable desorption of the dye, whose heat of adsorption is only about 190.8 kJ mol^{-1} [56]. However, Fig. 2d shows, that the amount of N719 dye in the mesoporous TiO_2 layer after treatment with PVBA or P4VP solutions remains practically at the same level of 0.15 mg/cm^2, as in the case of pure dye loading (i.e. without co-adsorbents when the concentration of polymers is zero).

This observation contrasts with the frequently observed decrease in dye loading when co-adsorbents are added [39]. On the one hand, the invariant dye loading is beneficial for photogeneration because the amount of sensitizer is at the highest possible level, which is determined by the surface area of the neat TiO_2. On the other hand, this may indicate a failure in the co-adsorption, which means that the polymers are not bound to the photoanode. The FTIR spectroscopy study refuted the latter and showed IR signals of PVBA and P4VP on titania with pre-adsorbed N719 (Fig. 3).

IR-spectrum of anatase powder with N719 dye displays several well-

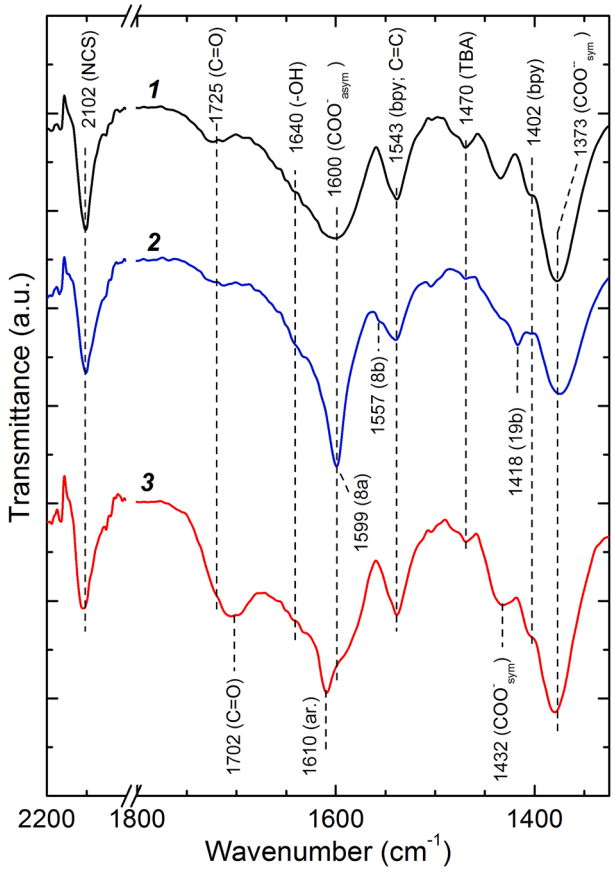

Fig. 3. FTIR spectra of anatase nanoparticles with adsorbed N719 dye (***1***), N719 dye with co-adsorbed P4VP (***2***) or PVBA (***3***).

distinguished bands assigned to symmetric vibration of COO^-_{sym} (1373 cm^{-1}), 2,2′-Bipyridine (bpy) moiety (1402 cm^{-1}), TBA ion (1470 cm^{-1}), C═C in bpy (1543 cm^{-1}), asymmetric vibration of COO^-_{asym} (1600 cm^{-1}), carbonyl C═O (1725 cm^{-1}) and NCS group (2100 cm^{-1}) [57]; a shoulder at 1640 cm^{-1} in the band of COO^-_{asym} is due to -OH vibrations on the TiO_2 surface [58]. Anchoring of N719 to TiO_2 via carboxylate groups causes a reduction of C═O band intensity with the appearance of COO^-_{asym} and COO^-_{sym} vibrations; the symmetric carboxylate vibrations point to covalent bonding of the dye to TiO_2 [57,59].

Co-adsorption of P4VP manifests itself as a strong band of 8a in-plane vibrational mode of the pyridine ring at 1599 cm^{-1}; this band overlaps with COO^-_{asym} of the dye at 1600 cm^{-1} and the overall intensity is much increased compared to the dye alone. Bands at 1557 and 1418 cm^{-1} are assigned to the pyridine 8a and 19b vibrational modes, respectively [60, 61]. The formation of coordinative bonding between N atom in the pyridine unit and the Lewis-acid centers of TiO_2 is monitored by 1615 cm^{-1} vibration, which appears when P4VP is adsorbed on titania [62]. Upon adsorption with dye, this band is affected and overlaps with COO^-_{asym} vibration of the dye carboxylic group, leading to a slight shoulder on the FTIR spectrum. Details on P4VP adsorption and FTIR spectra interpretation were addressed in a previous study [45].

IR-signals of PVBA appear at 1702 and 1610 cm^{-1}, which are due to vibrations of C═O group and aromatic ring, respectively [63,64]; the band at 1432 cm^{-2} was assigned to COO^-_{sym} stretching vibrations of carboxylic group complexed with Ti centers [65]. The pronounced band of C═O vibration at 1702 cm^{-1} indicates that part of the carboxylic groups in the adsorbed PVBA remains protonated. Increased (compared to the dye adsorption) band at 1600 cm^{-1} shows that part of the dissociated carboxylic groups of the PVBA are not bonded to titania. This observation can suggest that only a specific amount of the carboxylic

groups in PVBA molecule participate in anchoring to titania; the rest are in protonated and deprotonated forms.

Co-adsorption of the polymers affects the light absorbance spectra of the photoanode (Fig. 4); more pronouncedly in the case of P4VP.

The optical band corresponding to metal-ligand charge transfer [66] at 532 nm shifts to 520 nm after exposure to the P4VP solution. The blue shift of the absorption maxima is due to the promotion of dye anchoring to the TiO_2; the Brønsted base P4VP facilitates the esterification of the carboxylic groups with the titania surface [45]. Unlike P4VP, acidic by its acidic PVBA groups practically do not affect the band at 532 nm (Fig. 4), implying that the dye retains its original mode of anchoring to TiO_2.

3.2. Photovoltaic performance of DSSCs devices

The polymer concentration for sequential co-adsorption must be carefully optimized to achieve an optimum balance between suppressing recombination of back electrons and generating photocurrent. Insufficient polymer absorption results in a lack of recombination suppression. Excessive polymer adsorption hinders dye regeneration and reduces photocurrent; a P4VP concentration of 30 μM yields devices with the highest photovoltaic performance [45]. A half PVBA concentration of 15 μM results in the highest performing cells. (**Fig. S5, Table S2**). For convenience, the following discussions refer to DSSCs devices with photoanodes treated with 30 and 15 μM of P4VP and PVBA, respectively, i.e., optimized with each co-adsorbent.

Fig. 5 presents photo and dark current-potential (*I–V*) responses of the DSSCs with pristine TiO_2/N719 photoanodes and treated in P4VP or PVBA solutions. The photovoltaic metrics of the devices were extracted from the photocurrent-potential response and summarized in Table 1.

The total 1-Sun equivalent PCE is 8.3 % and 9.0 % for the cells with PVBA and P4VP-treated photoanodes, respectively (Table 1). The

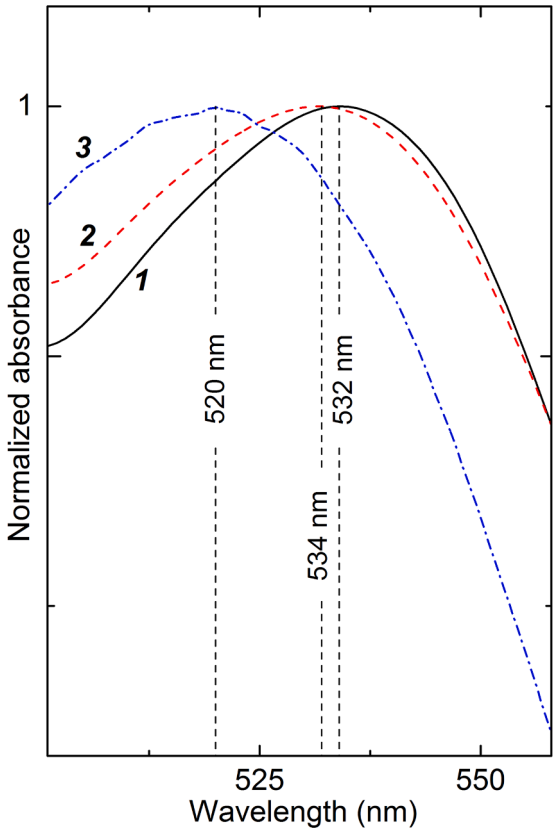

Fig. 4. Normalized absorption of the mesoporous TiO_2 film with neat N719 dye (***1***) and after sequential co-adsorption with PVBA (***2***) and P4VP (***3***).

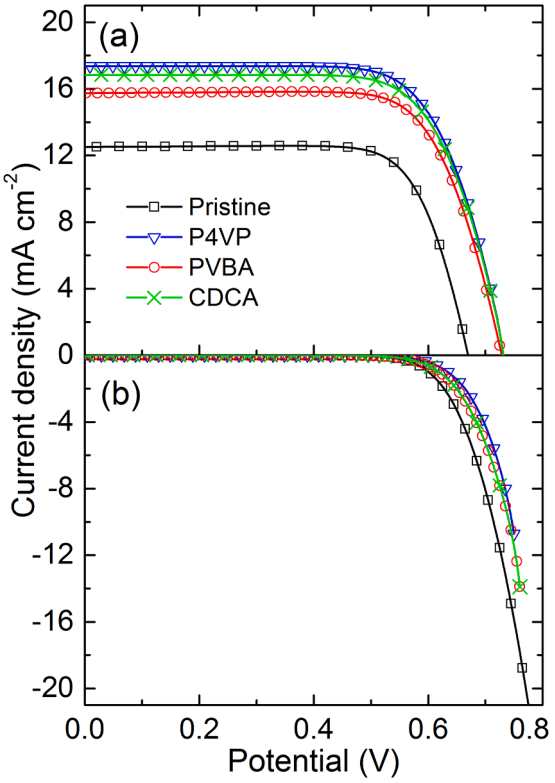

Fig. 5. *I-V* curves under 1- Sun equivalent (***a***) and in the dark (***b***) of the DSSCs with pristine TiO_2/dye photoanode (squares); after co-adsorbtion of P4VP (triangles), PVBA (circles) or CDCA (crosses).

Table 1
Photovoltaic metrics of DSSCs with pristine TiO_2/N719 photoanodes passivated with CDCA, and loaded with P4VP or PVBA co-adsorbents (* - PCE of the best performing device).

Photoanode	V_{oc} (V)	J_{sc} (mA cm^{-2})	FF	PCE (%)	J_{sc} from IPCE (mA cm^{-2})	Dye loading, (mg cm^{-2})
N719 (pristine)	0.67 ±0.01	12.5 ±0.1	0.75 ±0.01	6.3 ±0.2 (*6.5)	9.4	0.159 ±0.002
N719 + CDCA	0.73 ±0.01	16.8 ±0.1	0.71 ±0.01	8.8 ±0.2 (*8.9)	12.6	0.154 ±0.002
N719 + PVBA	0.73 ±0.01	15.7 ±0.2	0.72 ±0.01	8.3 ±0.2 (*8.5)	11.8	0.151 ±0.002
N719 + P4VP	0.73 ±0.01	17.4 ±0.2	0.71 ±0.01	9.0 ±0.1 (*9.1)	13.1	0.159 ±0.002

devices outperform those with pristine TiO_2/N719 photoanode, displaying a PCE of 6.3 %. It should be noted, that champion CDCA-passivated counterparts in the optimized device configuration and similar materials as in this study can deliver PCE of *ca.* 9.5 % [43,44]. In this work, CDCA-cells routinely displayed under simulated 1-Sun illumination, in an average of 4 devices, 8.8 % of PCE.

Upon P4VP, PVBA or CDCA adsorption the open circuit potential (V_{OC}) is improved by *ca.* 60 mV, which is due to suppressed dark currents (Fig. 5b). The primary factor influencing the PCE is the augmentation of saturation photocurrent (Fig. 5a) and short circuit current density (J_{SC}). The amount of loaded dye is consistently the same across all co-adsorbents studied (Table 1). The observed increase of the photocurrent is driven by co-adsorbents rather than the amount of the

absorbed dye. Fig. 6 presents incident photon conversion efficiency spectra (IPCE) of the devices. The IPCE onset below 760 nm corresponds to the transition from N719 ground state to the lowest excited state of the dye localized on TiO_2 (1.58 eV) [67]. The maximum at 528 nm of the pristine TiO_2/N719 fits well with optical absorption band of N719 in solution centered in 520 nm; the band is 8 nm positively shifted due to dye-TiO_2 coupling and delocalization of the excited electron into the semiconductor [68]. The shift is even more noticeable in the case of P4VP, PVBA, or CDCA-treated photoanodes, with the peak in IPCE occurring at ca. 536 nm, indicating stronger dye-TiO_2 anchoring; IPCE improves at wavelengths from 450 to 750 nm.

The calculated from IPCE spectra J_{SC} is consistent with those determined from *I-V* curves (Table 1). Still, it displays expectedly lower (*ca.* 25 %) values due to reflection and absorption losses of light on FTO glass [69] and is more impacted by the lagged response of DSSCs to the chopped monochromatic light [70].

Time-Correlated Single Photon Counting (TCSPC) experiments were performed in order to evaluate the dye excited states lifetime in the self-assembled monolayer without and with the presence of the new polymers P4VP and PVBA (Fig. 7). Two contributions to the decay are systematically observed with comparable amplitude between the two components. The fast component, in the range of 4 ns, is attributed to the partial charge injection of the excited dye into the TiO_2 nanocrystals. The longer component, of *ca.* 30 ns, is ascribed to the radiative decay of the dye on the self-assembled monolayer. Interestingly the results show that the introduction of the polymer modifies the overall kinetic without modifying the relative amplitude. It shows a slight acceleration of the charge injection when P4VP and PVBA are introduced, whereas the polymer enables prolonging the dye excited states to 40 ns with P4PV. The fitting results, using a classical two exponential components as mathematical function, are tabulated in Table 2. These results reveal on one hand that the presence of the polymer influences the dye packing within the self-assembled monolayer (SAM) in good agreement with other results herein presented, and on the other hand that molecular dye aggregation in the SAM, which typically accelerates the dye excited state lifetime, is herein hampered by the introduction of P4VP or PVBA, thus in good agreement with the greater device performances under low dim and AM1.5G conditions.

Following the emerging demand for converting low-intensity light in residential and working interiors, the photovoltaic performance of the DSSCs has also been determined under artificial indoor light (Fig. 8).

The *I-V* characteristics at low-light show the typical behavior of photodiode. At 500 lx, the cells enable the generation of the maximum output power of 25.5 and 32.1 μW cm^{-2} with PCEs of 17.5 % and 22.0 %

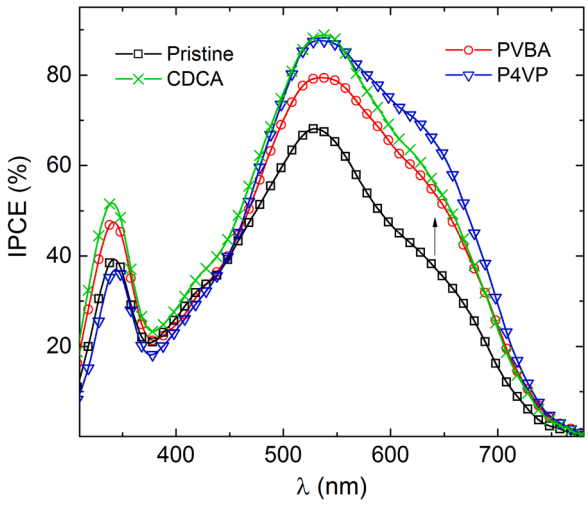

Fig. 6. IPCE spectra of DSSCs with pristine photoanode and treated with CDCA, PVBA or P4VP co-adsorbents.

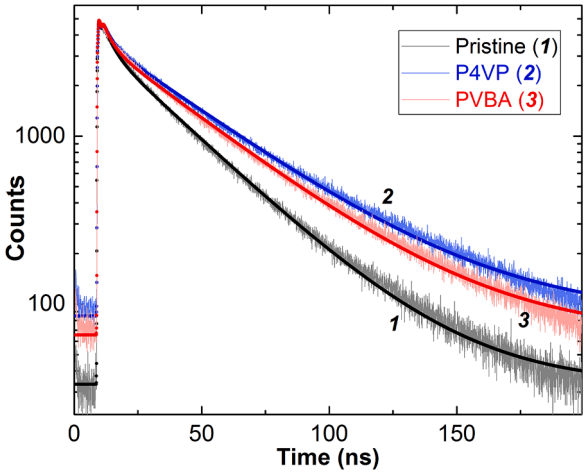

Fig. 7. Comparison of the time-resolved photoluminescence decay between reference cell (in black), and devices including P4VP (in blue) and PVBA (in red) polymers after excitation pulse at 475 nm with 4 nJ·cm^{-2} energy (emission probed at 770 nm). The fit results using bi-exponential function is represented in bold lines.

Table 2
Results from PL decay fitting of the different devices using a bi-exponential function. The half-time and amplitude of the two contributions are reported.

Photoanode	t_1 (ns)	A_1	t_2 (ns)	A_2
Pristine	3.963 (± 0.005)	0.0564 (± 0.0006)	30.343 (± 0.001)	0.0900 (± 0.0003)
P4PV	3.730 (± 0.006)	0.0502 (± 0.0007)	40.055 (±0.001)	0.0939 (± 0.0003)
PVBA	3.523 (± 0.006)	0.0570 (± 0.0007)	37.418 (±0.001)	0.0923 (± 0.0002)

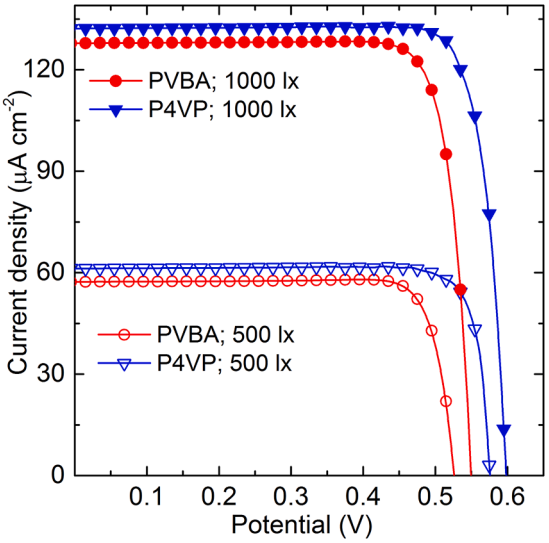

Fig. 8. *I–V* curves of the DSSCs with P4VP (triangles) and PVBA (circles) treated photoanodes under 500 lx (empty symbols) and 1000 lx (full symbols) LED light.

using PVBA and P4VP as co-adsorbents, respectively. Increasing the light intensity twofold doubled the photocurrent and improved V_{OC}, as expected. At 1000 lx, a maximum output power of 58.2 and 69.1 μW cm^{-2} and PCE of 18.8 % and 22.4 % were obtained with PVBA and P4VP-loaded photoanodes, respectively. These PCE values for artificial light and maximum output power in relatively common devices using

the N719 dye and new polymeric co-adsorbents are competing or surpassing more sophisticated counterparts using toxic cobalt electrolytes and untrivial dyes [5].

The observed increase in photocurrent and higher V_{OC} after polymer adsorption are also due to the suppression of back electron recombination in the devices, as revealed by the EIS study (Fig. 9a). Another reasons for the higher photocurrents is the promotion of dye anchoring to TiO_2, which is evident in a blue shift of the metal-ligand charge transfer optical band at *ca.* 532 nm (Fig. 4), improvement of charge injection and excited dye lifetime (Fig. 7, Table 2).

Nyquist plots of the devices with untreated TiO_2/N719 and the photoanode passivated with polymers show two well-distinguishable capacitive semicircles. The radii of the smaller and larger semicircles reflect the resistances of electron transfer at the interfaces of the counter-electrode and photoanode with the electrolyte, respectively [71]. The equivalent circuit in Fig. 9b fits well with the impedance spectra. CPE_{CE} and CPE_K are the constant phase elements at the counter-electrode/electrolyte and photoanode/electrolyte interfaces, respectively. The charge transfer resistances at the counter-electrode/electrolyte interface (R_{CE}), at the photoanode/electrolyte interface (R_K) and the series resistance (R_S) were obtained by fitting the model to the impedance spectra (Table 3).

As expected, the resistances R_S and R_{CE} are practically unaffected by the adsorption of polymer on the photoanode. The resistance R_K is significantly increased by the polymer loading which is related to the suppression of recombination of back-electron with triiodide ions. Cells with P4VP show slightly higher R_K values than their counterparts with co-adsorbed PVBA, leading to better J_{SC} when compared to PVBA counterparts (Fig. 5a).

The recombination losses at the PVBA-treated photoanode can be further reduced (R_K can be increased) by using higher polymer concentrations are used in the co-adsorption solution, as suggested by the EIS study of the devices prepared with different PVBA concentrations (**Fig. S6, Table S3**). Although the R_K value increases at PVBA concentrations above 15 μM (**Table S3**), the overall photocurrent is compromised (**Fig. S5, Table S2**). This trend is due to the excessive adsorption of PVBA, which leads to the formation of PVBA molecular layers above the adsorbed dye and hinders dye regeneration. A pronounced C=O vibration band at 1702 cm^{-1} in the IR spectrum (Fig. 3) indicates multilayer adsorption, whereas this band should be blurred and disappear in the case of monolayer and dissociative adsorption of the benzoic acid fragment band [64].

An interesting approach for further PCE improvement can be combining N719 and CDCA co-adsorption followed by sequential adsorption of P4VP or PVBA; however, it leads to the underperforming devices with low FF (**Fig. S7, Table S4**).

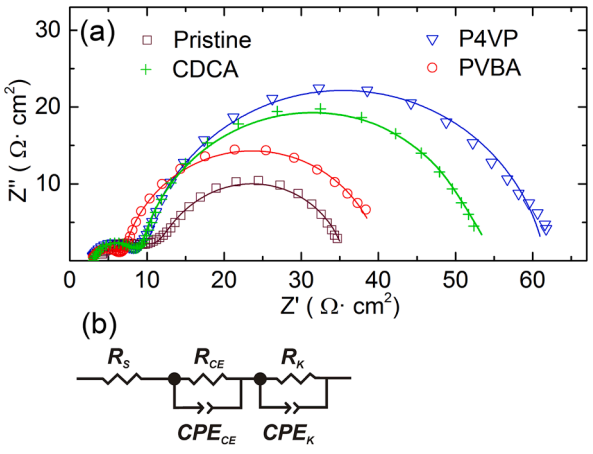

Fig. 9. Nyquist diagrams for DSSCs with pristine TiO_2/N719 photoanode (squares); passivated with P4VP (triangles), PVBA (circles) or CDCA (crosses) (***a***). Solid lines show the fittings to the equivalent circuit model (***b***).

Table 3
Internal resistances of DSSCs with pristine TiO_2/N719 photoanode and passivated with PVBA and P4VP co-adsorbents.

Photoanode	R_S (Ω cm^2)	R_{CE} (Ω cm^2)	R_K (Ω cm^2)
N719 (pristine)	3.2	9.1	23.5
N719 + CDCA	3.0	6.1	44.7
N719 + PVBA	2.8	4.2	33.4
N719 + P4VP	2.7	6.6	52.4

3.3. *Long-term stability of the DSSCs devices*

The effects of P4VP and PVBA co-adsorbents on the long-term stability of cells in the light soaking test according to the ISOS-L2 protocol were investigated in fully glass-encapsulated devices (Fig. 1) using 3-methoxypropionitrile-based iodine electrolyte. This electrolyte has a low volatility and a high concentration of triiodide ions making its use relevant to the evaluation of the long-term operation. However, it leads to devices with lower PCE – a disadvantage arising from a reasonable balance between high initial PCE and good stability [72].

For comparison, cells with photoanodes passivated with the conventional co-adsorbent CDCA were tested under the same conditions. **Fig. S8** shows representative *I-V* curves of the devices at the beginning of the aging test; detailed photovoltaic readings are summarized in **Table S5**. At the beginning of the light soaking test, the PCE values of the cells with the co-adsorbents, CDCA, P4VP, and PVBA were 4.9 ± 0.2 %, 4.1 ± 0.2 %, and 4.3 ± 0.2 %, respectively. The initial PCEs values of the devices are reasonably comparable, are within the normal scatter of experimental data values, and are sufficient to estimate the effect of the recombination-suppressing additive on the degradation rate.

Devices with CDCA co-adsorbent show the most stable PCE metrics with slightly improved overall PCE due to meliorating of J_{SC} and FF after *ca.* 200 h of light soaking (Fig. 10). High stability of CDCA-treated devices originates from strong bonding of CDCA to titania; determined activation energy for the CDCA adsorption on TiO_2 is 68.9 kJ mol^{-1} [73], clearly signifying chemical bonding.

Considering the total PCE (Fig. 10a), the cells with PVBA co-adsorbent showed the most steady-state similar to their CDCA counterparts. After 1000 h of continuous operation with passive load, devices with CDCA and PVBA passivated photoanodes show very close and low PCE degradation rates of $1.5{\cdot}10^{-3}$ and $1.6{\cdot}10^{-3}$ per day, respectively. A continuous decrease in of the FF of PVBA cells is compensated by an improved V_{OC} (Fig. 10c) and slightly increasing J_{SC}. Cells with P4VP co-adsorbent show the opposite and sharply decreasing trend of PCE with a deterioration rate up to $12.1{\cdot}10^{-3}$ per day. The loss of photovoltaic performance of P4VP cells is obviously due to decreasing J_{SC} and FF, as shown in Fig. 10b,d.

The observed disparity in stability between devices with P4VP and PVBA can be attributed to the distinct polymer structures (as illustrated in Fig. 2a and b). Specifically, this distinction arises from the functional groups within these polymers that have the potential to interact with the TiO_2 surface. Carboxylic acid groups display a notable chemical affinity for the titania surface and are capable of forming ester-like bonds, bidentate bridges, or bidentate chelates with Ti surface centers, as previously documented [74]. In contrast, the adsorption of pyridine groups is notably weaker [75] and primarily occurs through coordinative bonding between the nitrogen heteroatom and the Lewis acid sites of titania [45,60,61,75]. The calculated heats of adsorption of benzoic acid and pyridine on anatase TiO_2 of about 96-136 kJ mol^{-1} [76] and 36-90 kJ mol^{-1} [77], respectively, support these facts. The excellent long-term stability of devices with PVBA co-adsorbent can be attributed to the strong binding of the polymer to the TiO_2 surface. At the same time, P4VP is likely to be desorbed from the titanium dioxide, opening the way for the recombination of back electrons, as shown by the decrease in

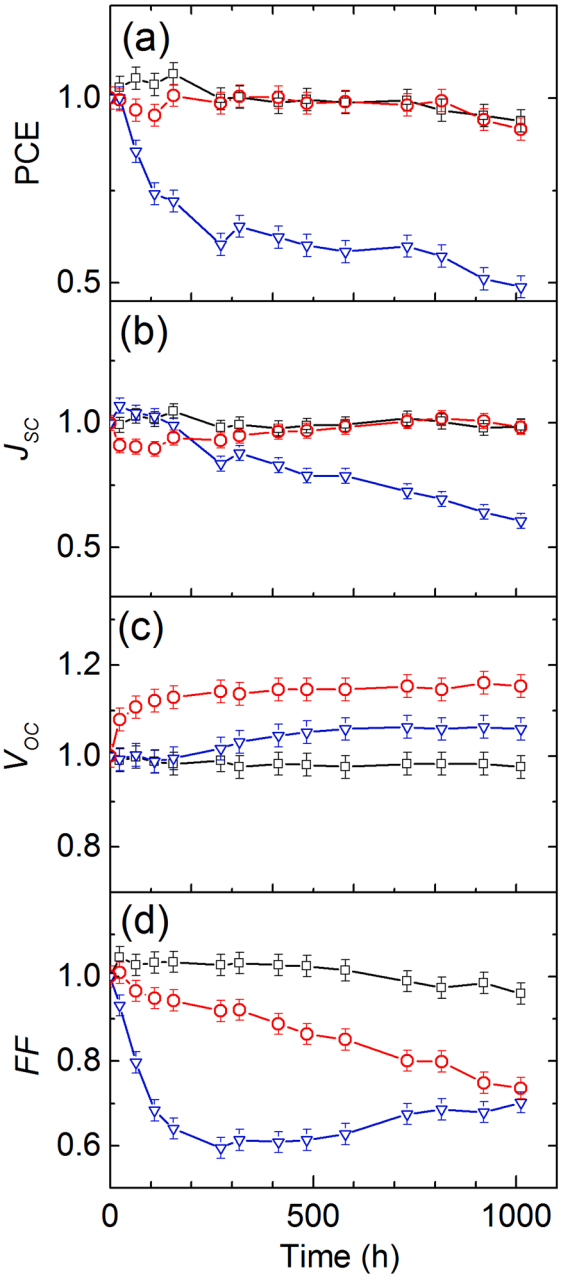

Fig. 10. Normalized PCE (***a***), J_{SC} (***b***), V_{OC} (***c***), and FF (***d***) of the devices with photoanodes passivated by CDCA (squares), P4VP (triangles), or PVBA (circles) co-adsorbents.

J_{SC} (Fig. 10b). However, the observed decrease in FF in PVBA passivated devices (Fig. 10d) could affect PCE under much longer or more stringent test conditions, which could be investigated in future studies.

4. Conclusions

The homopolymers P4VP and PVBA with narrow and controlled molecular weight distribution prepared by RAFT polymerization are new promising fully synthetic recombination suppressors. When adsorbed with N719, the polymers do not cause unwanted dye desorption and significantly restrain reverse current by increasing the recombination resistance at the photoanode/electrolyte interface; V_{OC} and J_{SC} are improved compared to the devices with pristine photoanodes.

Time-Correlated Single Photon Counting showed an acceleration of the charge injection and prolonging the dye excited states when P4VP and PVBA are co-adsorbed with N719.

Under carefully optimized co-adsorption conditions, P4VP and PVBA yielded devices with 1-Sun PCE of 9.0 % and 8.3 %, respectively, strongly competitive with CDCA-passivated counterparts that have PCE of about 8.8 %. Under 1000 lx LED light, indoor PVBA and P4VP cells yielded good output power of 58.2 and 69.1 μW cm^{-2} with PCE of 18.8 % and 22.4 %, respectively, which is suitable for use as indoor PVs.

The long-term PCE stability of P4VP- and PVBA-passivated cells was evaluated in glass-encapsulated devices with the highest ever possible degree of hermeticity; which is vital for reliable decoupling intrinsic and extrinsic degradation factors. Under 1000 h of continuous light exposure with passive resistance load according to ISOS-L2 protocol, DSSCs with PVBA-treated photoanodes showed equivalent stability to their CDCA-counterparts with similar deterioration factors. DSSCs with P4VP-passivated photoanodes showed poor PCE stability due to the rapid photocurrent degradation and poor bonding of co-adsorbent to the titanium dioxide. The excellent stability of PVBA devices is of course due to the polymer structure, which is rich in carboxyl groups; the latter ensures the stability of the adsorbed polymer layer on titanium dioxide due to a stronger chemical bonding. The fully synthetic PVBA co-adsorbent provides good device PCE and ISOS-L2 stability, which is of interest as a fully thynsetic, animal by-product free alternative to CDCA for commercial production.

Declaration of Competing Interest

The authors declare that they have no known competing financial interests or personal relationships that could have appeared to influence the work reported in this paper.

Data availability

Data will be made available on request.

Acknowledgments

Daniela Rodrigues acknowledges the FCT– Fundação para a Ciência e a Tecnologia for her doctoral grants SFRH/BD/131818/2017 and COVID/BD/152163/2021. J. Martins acknowledges the FCT for his doctoral grant SFRH/BD/119402/2019. This work was financially supported by LA/P/0045/2020 (ALiCE), UIDB/00511/2020, and UIDP/00511/2020 (LEPABE), funded by national funds through FCT/MCTES (PIDDAC). Project 2SMART – engineered Smart materials for Smart citizens, with the reference NORTE-01-0145-FEDER-000054, under the Portugal 2020 Partnership Agreement, through the European Regional Development Fund (ERDF). National funds through FCT, under the project UIDB/00285/2020 and LA/P/0112/2020. NMR data was collected at the UC-NMR facility which is supported in part by FEDER – through the COMPETE and FCT – grants REEQ/481/QUI/2006, RECI/QEQ QFI/0168/2012, CENTRO-07-CT62-FEDER-002012, and Rede Nacional de Ressonância Magnética Nuclear (RNRMN). Carlos M. R. Abreu wishes to thank FCT for his grant CEECIND/03591/2018. Alliance for Energy Transition (ATE) N. C644914747-00000023, project 56 of the Incentive System “Agendas for Business Innovation”, financed by the Recovery and Resilience Plan (PRR) and by European Funds Next-Generation EU.

Supplementary materials

Supplementary material associated with this article can be found, in the online version, at doi:10.1016/j.surfin.2023.103627.

References

[1] A.B. Muñoz-García, I. Benesperi, G. Boschloo, J.J. Concepcion, J.H. Delcamp, E. A. Gibson, G.J. Meyer, M. Pavone, H. Pettersson, A. Hagfeldt, M. Freitag, Dye-sensitized solar cells strike back, Chem. Soc. Rev. 50 (2021) 12450–12550, https://doi.org/10.1039/D0CS01336F.

[2] N. Mariotti, M. Bonomo, L. Fagiolari, N. Barbero, C. Gerbaldi, F. Bella, C. Barolo, Recent advances in eco-friendly and cost-effective materials towards sustainable dye-sensitized solar cells, Green Chem. 22 (2020) 7168–7218, https://doi.org/10.1039/D0GC01148G.

[3] M. Kokkonen, P. Talebi, J. Zhou, S. Asgari, S.A. Soomro, F. Elsehrawy, J. Halme, S. Ahmad, A. Hagfeldt, S.G. Hashmi, Advanced research trends in dye-sensitized solar cells, J. Mater. Chem. A 9 (2021) 10527–10545, https://doi.org/10.1039/D1TA00690H.

[4] D. Zhang, M. Stojanovic, Y. Ren, Y. Cao, F.T. Eickemeyer, E. Socie, N. Vlachopoulos, J.-E. Moser, S.M. Zakeeruddin, A. Hagfeldt, M. Grätzel, A molecular photosensitizer achieves a V_{OC} of 1.24 V enabling highly efficient and stable dye-sensitized solar cells with copper(II/I)-based electrolyte, Nat. Commun. 12 (2021) 1777, https://doi.org/10.1038/s41467-021-21945-3.

[5] Y. Ren, D. Zhang, J. Suo, Y. Cao, F.T. Eickemeyer, N. Vlachopoulos, S. M. Zakeeruddin, A. Hagfeldt, M. Grätzel, Hydroxamic acid preadsorption raises efficiency of cosensitized solar cells, Nature 613 (2022) 60–65, https://doi.org/10.1038/s41586-022-05460-z.

[6] H. Yuan, W. Wang, D. Xu, Q. Xu, J. Xie, X. Chen, T. Zhang, C. Xiong, Y. He, Y. Zhang, Y. Liu, H. Shen, Outdoor testing and aging of dye-sensitized solar cells for building integrated photovoltaics, Sol. Energy 165 (2018) 233–239, https://doi.org/10.1016/j.solener.2018.03.017.

[7] J. Barichello, L. Vesce, P. Mariani, E. Leonardi, R. Braglia, A. Di Carlo, A. Canini, A. Reale, Stable semi-transparent dye-sensitized solar modules and panels for greenhouse application, Energies 14 (2021) 6393, https://doi.org/10.3390/en14196393.

[8] M. Bonomo, A.Y.S. Zarate, L. Fagiolari, A. Damin, S. Galliano, C. Gerbaldi, F. Bella, C. Barolo, Unreported resistance in charge transport limits the photoconversion efficiency of aqueous dye-sensitised solar cells: an electrochemical impedance spectroscopy study, Mater. Today Sustain. 21 (2023), 100271, https://doi.org/10.1016/j.mtsust.2022.100271.

[9] J.C. De Haro, E. Tatsi, L. Fagiolari, M. Bonomo, C. Barolo, S. Turri, F. Bella, G. Griffini, Lignin-based polymer electrolyte membranes for sustainable aqueous dye-sensitized solar cells, ACS Sustain. Chem. Eng. 9 (2021) 8550–8560, https://doi.org/10.1021/acssuschemeng.1c01882.

[10] M. Wu, X. Zhao, J. Gao, J. Guo, J. Xiao, R. Chen, Multifunctional boron-doped carbon fiber electrodes synthesized by electrospinning for supercapacitors, dye-sensitized solar cells, and photocapacitors, Surf. Interfaces 31 (2022), 101983, https://doi.org/10.1016/j.surfin.2022.101983.

[11] T. da Silva Lopes, P. Dias, R. Monteiro, A. Vilanova, D. Ivanou, A. Mendes, A 25 cm^2 solar redox flow cell: facing the engineering challenges of upscaling, Adv. Energy Mater. 12 (2021), 2102893, https://doi.org/10.1002/aenm.202102893.

[12] A. Khataee, J. Azevedo, P. Dias, D. Ivanou, E. Dražević, A. Bentien, A. Mendes, Integrated design of hematite and dye-sensitized solar cell for unbiased solar charging of an organic-inorganic redox flow battery, Nano Energy 62 (2019) 832–843, https://doi.org/10.1016/j.nanoen.2019.06.001.

[13] S.H. Kang, M.J. Jeong, Y.K. Eom, I.T. Choi, S.M. Kwon, Y. Yoo, J. Kim, J. Kwon, J. H. Park, H.K. Kim, Porphyrin sensitizers with donor structural engineering for superior performance dye-sensitized solar cells and tandem solar cells for water splitting applications, Adv. Energy Mater. 7 (2017) 1–10, https://doi.org/10.1002/aenm.201602117.

[14] S.J. Varma, K.S. Kumar, S. Seal, S. Rajaraman, J. Thomas, Fiber-type solar cells, nanogenerators, batteries, and supercapacitors for wearable applications, Adv. Sci. 5 (2018), 1800340, https://doi.org/10.1002/advs.201800340.

[15] T.M.W.J. Bandara, J.M.C. Hansadi, F. Bella, A review of textile dye-sensitized solar cells for wearable electronics, Ionics (Kiel) 28 (2022) 2563–2583, https://doi.org/10.1007/s11581-022-04582-8.

[16] J.H. Kim, S.J. Koo, H. Cho, J.W. Choi, S.Y. Ryu, J.W. Kang, S.H. Jin, C. Ahn, M. Song, 6.16% Efficiency of solid-state fiber dye-sensitized solar cells based on LiTFSI electrolytes with novel TEMPOL derivatives, ACS Sustain. Chem. Eng. 8 (2020) 15065–15071, https://doi.org/10.1021/acssuschemeng.0c05427.

[17] H. Zheng, D. Li, C. Ran, Q. Zhong, L. Song, Y. Chen, P. Müller-Buschbaum, W. Huang, Emerging organic/hybrid photovoltaic cells for indoor applications: recent advances and perspectives, Solar RRL 5 (2021), 2100042, https://doi.org/10.1002/solr.202100042, 5.

[18] S. Venkatesan, W.-H. Lin, T.-H. Hsu, H. Teng, Y.-L. Lee, Indoor dye-sensitized solar cells with efficiencies surpassing 26% using polymeric counter electrodes, ACS Sustain. Chem. Eng. 10 (2022) 2473–2483, https://doi.org/10.1021/acssuschemeng.1c07626.

[19] M.A. Saeed, K. Yoo, H.C. Kang, J.W. Shim, J.-J. Lee, Recent developments in dye-sensitized photovoltaic cells under ambient illumination, Dyes Pigm. 194 (2021), 109626, https://doi.org/10.1016/j.dyepig.2021.109626.

[20] H. Michaels, M. Rinderle, R. Freitag, I. Benesperi, T. Edvinsson, R. Socher, A. Gagliardi, M. Freitag, Dye-sensitized solar cells under ambient light powering machine learning: towards autonomous smart sensors for the internet of things, Chem. Sci. 11 (2020) 2895–2906, https://doi.org/10.1039/C9SC06145B.

[21] Y. Cao, Y. Liu, S.M. Zakeeruddin, A. Hagfeldt, M. Grätzel, Direct contact of selective charge extraction layers enables high-efficiency molecular photovoltaics, Joule 2 (2018) 1108–1117, https://doi.org/10.1016/j.joule.2018.03.017.

[22] M. Aftabuzzaman, S. Sarker, C. Lu, H.K. Kim, In-depth understanding of the energy loss and efficiency limit of dye-sensitized solar cells under outdoor and indoor conditions, J. Mater. Chem. A 9 (2021) 24830–24848, https://doi.org/10.1039/D1TA03309C.

[23] A. Aslam, U. Mehmood, M.H. Arshad, A. Ishfaq, J. Zaheer, A. Ul Haq Khan, M. Sufyan, Dye-sensitized solar cells (DSSCs) as a potential photovoltaic technology for the self-powered internet of things (IoTs) applications, Sol. Energy 207 (2020) 874–892, https://doi.org/10.1016/j.solener.2020.07.029.

[24] A.J. Frank, N. Kopidakis, J. Van de Lagemaat, Electrons in nanostructured TiO_2 solar cells: transport, recombination and photovoltaic properties, Coord. Chem. Rev. 248 (2004) 1165–1179, https://doi.org/10.1016/j.ccr.2004.03.015.

[25] K. Sharma, V. Sharma, S.S. Sharma, Dye-sensitized solar cells: fundamentals and current status, Nanoscale Res. Lett. 13 (2018) 381–427, https://doi.org/10.1186/s11671-018-2760-6.

[26] V.S. Manthou, E.K. Pefkianakis, P. Falaras, G.C. Vougioukalakis, Co-adsorbents: a key component in efficient and robust dye-sensitized solar cells, ChemSusChem 8 (2015) 588–599, https://doi.org/10.1002/cssc.201403211.

[27] N.R. Neale, N. Kopidakis, J. Van de Lagemaat, M. Grätzel, A.J. Frank, Effect of a coadsorbent on the performance of dye-sensitized TiO_2 solar cells: shielding versus band-edge movement, J. Phys. Chem. B. 109 (2005) 23183–23189, https://doi.org/10.1021/jp0538666.

[28] L.F.G. Larsson, G.T. Tractz, A.P. Camargo Matheus, P.R. Pinto Rodrigues, The use of 2-mercaptobenzothiazole as a new Co-adsorbent in dye-sensitized solar cells, Opt. Mater. (Amst). 131 (2022), 112658, https://doi.org/10.1016/j.optmat.2022.112658.

[29] H.M. Song, K.D. Seo, M.S. Kang, I.T. Choi, S.K. Kim, Y.K. Eom, J.H. Ryu, M.J. Ju, H. K. Kim, A simple triaryl amine-based dual functioned co-adsorbent for highly efficient dye-sensitized solar cells, J. Mater. Chem. 22 (2012) 3786–3794, https://doi.org/10.1039/c2jm16021h.

[30] B.J. Song, H.M. Song, I.T. Choi, S.K. Kim, K.D. Seo, M.S. Kang, M.J. Lee, D.W. Cho, M.J. Ju, H.K. Kim, A desirable hole-conducting coadsorbent for highly efficient dye-sensitized solar cells through an organic redox cascade strategy, Chem. - A Eur. J. 17 (2011) 11115–11121, https://doi.org/10.1002/chem.201100813.

[31] I.T. Choi, M.J. Ju, S.H. Song, S.G. Kim, D.W. Cho, C. Im, H.K. Kim, Tailor-made hole-conducting coadsorbents for highly efficient organic dye-sensitized solar cells, Chem. - A Eur. J. 19 (2013) 15545–15555, https://doi.org/10.1002/chem.201301658.

[32] A. Kay, M. Grätzel, Artificial Photosynthesis. 1. Photosensitization of TiO_2 Solar Cells with Chlorophyll Derivatives and Related Natural Porphyrins, J. Phys. Chem. 97 (1993) 6272–6277, https://doi.org/10.1021/j100125a029.

[33] K.M. Lee, C.Y. Chen, S.J. Wu, S.C. Chen, C.G. Wu, Surface Passivation: The Effects of CDCA Co-Adsorbent and Dye Bath Solvent on the Durability of Dye-Sensitized Solar Cells, Sol. Energy Mater. Sol. Cells 108 (2013) 70–77, https://doi.org/10.1016/j.solmat.2012.08.008.

[34] P. Salvatori, G. Marotta, A. Cinti, C. Anselmi, E. Mosconi, F. De Angelis, Supramolecular Interactions of Chenodeoxycholic Acid Increase the Efficiency of Dye-Sensitized Solar Cells Based on a Cobalt Electrolyte, J. Phys. Chem. C 117 (2013) 3874–3887, https://doi.org/10.1021/jp4003577.

[35] D. Friedrich, L. Valldecabres, M. Kunst, T. Moehl, S.M. Zakeeruddin, M. Grätzel, Dye Regeneration Dynamics by Electron Donors on Mesoscopic TiO_2 Films, J. Phys. Chem. C 118 (2014) 3420–3425, https://doi.org/10.1021/jp4113206.

[36] H. Trilaksana, C. Shearer, L. Kloo, G.G. Andersson, Restructuring of Dye Layers in Dye Sensitized Solar Cells: Cooperative Adsorption of N719 and Chenodeoxycholic Acid on Titania, ACS Appl. Energy Mater. 2 (2019) 124–130, https://doi.org/10.1021/acsaem.8b01864.

[37] W. Liu, H. Jiang, J. Shi, B. Lu, H. Cai, Z. Mao, F. Kong, In Situ Evaluation of Kinetics and Interaction Mechanism between Chenodeoxycholic Acid and N719 on Dye-Sensitized Nanofilm Surface, ACS Appl. Energy Mater. 3 (2020) 3310–3317, https://doi.org/10.1021/acsaem.9b02321.

[38] A.F. Hofmann, L.R. Hagey, Key Discoveries in Bile Acid Chemistry and Biology and Their Clinical Applications: History of the Last, J. Lipid Res. 55 (2014) 1553–1595, https://doi.org/10.1194/jlr.R049437.

[39] Y.G. Lee, S. Park, W. Cho, T. Son, P. Sudhagar, J.H. Jung, S. Wooh, K. Char, Y. S. Kang, Effective Passivation of Nanostructured TiO_2 Interfaces with PEG-Based Oligomeric Coadsorbents to Improve the Performance of Dye-Sensitized Solar Cells, J. Phys. Chem. C 116 (2012) 6770–6777, https://doi.org/10.1021/jp210360n.

[40] Y.G. Lee, D. Song, J.H. Jung, S. Wooh, S. Park, W. Cho, W. Wei, K. Char, Y.S. Kang, TiO_2 Surface Engineering with Multifunctional Oligomeric Polystyrene Coadsorbent for Dye-Sensitized Solar Cells, RSC Adv 5 (2015) 68413–68419, https://doi.org/10.1039/C5RA12889G.

[41] H. An, D. Song, J. Lee, E.M. Kang, J. Jaworski, J.M. Kim, Y.S. Kang, Promotion of Strongly Anchored Dyes on the Surface of Titania by Tetraethyl Orthosilicate Treatment for Enhanced Solar Cell Performance, J. Mater. Chem. A 2 (2014) 2250–2255, https://doi.org/10.1039/C3TA13152A.

[42] S.H. Park, J. Lim, I.Y. Song, N. Atmakuri, S. Song, Y.S. Kwon, J.M. Choi, T. Park, Stable Dye-Sensitized Solar Cells by Encapsulation of N719-Sensitized TiO_2 Electrodes Using Surface-Induced Cross-Linking Polymerization, Adv. Energy Mater. 2 (2012) 219–224, https://doi.org/10.1002/aenm.201100533.

[43] C. Hora, F. Santos, M.G.F. Sales, D. Ivanou, A. Mendes, Dye-Sensitized Solar Cells for Efficient Solar and Artificial Light Conversion, ACS Sustain. Chem. Eng. 7 (2019) 13464–13470, https://doi.org/10.1021/acssuschemeng.9b02990.

[44] C. Hora, F. Santos, M.G.F. Sales, D. Ivanou, A.M. Mendes, Conventional and Back-Illuminated Cobalt- and Iodine-Mediated Dye-Sensitized Solar Cells for Artificial and Solar Light Conversion, ACS Appl. Energy Mater. 5 (2022) 14846–14857, https://doi.org/10.1021/acsaem.2c02307.

[45] D.F.S.L. Rodrigues, F. Santos, C.M.R. Abreu, J.F.J. Coelho, A.C. Serra, D. Ivanou, A. Mendes, Passivation of the TiO_2 Surface and Promotion of N719 Dye Anchoring

with Poly(4-vinylpyridine) for Efficient and Stable Dye-Sensitized Solar Cells, ACS Sustain. Chem. Eng. 9 (2021) 5981–5990, https://doi.org/10.1021/acssuschemeng.1c00842.
[46] M.O. Reese, S.A. Gevorgyan, M. Jørgensen, E. Bundgaard, S.R. Kurtz, D.S. Ginley, D.C. Olson, M.T. Lloyd, P. Morvillo, E.A. Katz, A. Elschner, O. Haillant, T. R. Currier, V. Shrotriya, M. Hermenau, M. Riede, K.R. Kirov, G. Trimmel, T. Rath, O. Inganäs, F. Zhang, M. Andersson, K. Tvingstedt, M. Lira-Cantu, D. Laird, C. McGuiness, S. Gowrisanker, M. Pannone, M. Xiao, J. Hauch, R. Steim, D. M. Delongchamp, R. Rösch, H. Hoppe, N. Espinosa, A. Urbina, G. Yaman-Uzunoglu, J.B. Bonekamp, A.J.J.M. Van Breemen, C. Girotto, E. Voroshazi, F.C. Krebs, Consensus Stability Testing Protocols for Organic Photovoltaic Materials and Devices, Sol. Energy Mater. Sol. Cells 95 (2011) 1253–1267, https://doi.org/10.1016/j.solmat.2011.01.036.
[47] S. Perrier, 50th Anniversary Perspective: RAFT Polymerization -, Macromolecules 50 (2017) 7433–7447, https://doi.org/10.1021/acs.macromol.7b00767.
[48] C.M.R. Abreu, A.C. Fonseca, N.M.P. Rocha, J.T. Guthrie, A.C. Serra, J.F.J. Coelho, Poly(vinyl chloride) by reversible deactivation radical polymerization: current status and future perspectives, Prog. Polym. Sci. 87 (2018) 34–69, https://doi.org/10.1016/j.progpolymsci.2018.06.007.
[49] J. Martins, S. Emami, R. Madureira, J. Mendes, D. Ivanou, A. Mendes, Novel Laser-Assisted Glass Frit Encapsulation for Long-Lifetime Perovskite Solar Cells, J. Mater. Chem. A 8 (2020) 20037–20046, https://doi.org/10.1039/D0TA05583B.
[50] F. Santos, J. Martins, J. Capitão, S. Emami, D. Ivanou, A. Mendes, Stable Cobalt-Mediated Monolithic Dye-Sensitized Solar Cells by Full Glass Encapsulation, ACS Appl. Energy Mater. 5 (2022) 7220–7229, https://doi.org/10.1021/acsaem.2c00765.
[51] J. Martins, S. Emami, D. Ivanou, A. Mendes, Ultralow Temperature Glass Frit Encapsulation for Stable Dye-Sensitized Solar Cells, ACS Appl. Energy Mater. 5 (2022) 14185–14192, https://doi.org/10.1021/acsaem.2c02714.
[52] J. Capitão, J. Martins, S. Emami, D. Ivanou, A. Mendes, Fully Glass Frit Encapsulated Dye-Sensitized Solar Cells: Challenges for Hermetical Sealing of Electrolyte Injection Holes, Sol. Energy 249 (2023) 476–484, https://doi.org/10.1016/j.solener.2022.12.001.
[53] Test method standard microcircuits, United States Department of Defense, 2010.
[54] IEC61646. 2008 Thin-film terrestrial photovoltaic (PV) modules- design qualification and type approval.
[55] M.V. Khenkin, E.A. Katz, A. Abate, G. Bardizza, J.J. Berry, C. Brabec, F. Brunetti, V. Bulović, Q. Burlingame, A. Di Carlo, R. Cheacharoen, Y.-B. Cheng, A. Colsmann, S. Cros, K. Domanski, M. Dusza, C.J. Fell, S.R. Forrest, Y. Galagan, D. Di Girolamo, M. Grätzel, A. Hagfeldt, E. von Hauff, H. Hoppe, J. Kettle, H. Köbler, M.S. Leite, S. Liu, Y.-L. Loo, J.M. Luther, C.-Q. Ma, M. Madsen, M. Manceau, M. Matheron, M. McGehee, R. Meitzner, M.K. Nazeeruddin, A.F. Nogueira, Ç Odabaşı, A. Osherov, N.-G. Park, M.O. Reese, F. De Rossi, M. Saliba, U.S. Schubert, H.J. Snaith, S.D. Stranks, W. Tress, P. A. Troshin, V. Turkovic, S. Veenstra, I. Visoly-Fisher, A. Walsh, T. Watson, H. Xie, R. Yıldırım, S.M. Zakeeruddin, K. Zhu, M. Lira-Cantu, Consensus statement for stability assessment and reporting for perovskite photovoltaics based on ISOS procedures, Nat. Energy 5 (2020) 35-49. https://doi.org/10.1038/s41560-019-0529-5.
[56] B.M. Marwa, S. Bruno, B. Mongi, F. Tran Van, B.L. Abdelmottaleb, Modeling of Adsorption Isotherms of Dye N719 on Titanium Oxide Using the Grand Canonical Ensemble in, Statistical Physics for Dye Sensitized Solar Cells, Sol. Energy 135 (2016) 177–187, https://doi.org/10.1016/j.solener.2016.05.015.
[57] K.E. Lee, M.A. Gomez, S. Elouatik, G.P. Demopoulos, Further Understanding of the Adsorption Mechanism of N719 Sensitizer on Anatase TiO_2 Films for DSSC Applications Using Vibrational Spectroscopy and Confocal Raman Imaging, Langmuir 26 (2010) 9575–9583, https://doi.org/10.1021/la100137u.
[58] P.A. Connor, K.D. Dobson, A.J. McQuillan, Infrared Spectroscopy of the TiO_2/Aqueous Solution Interface, Langmuir 15 (1999) 2402–2408, https://doi.org/10.1021/la980855d.
[59] A. Amini, M.S. Zakerhamidi, S. Khorram, Treatment of the ZnO and TiO_2 Thin Films by Electric Field in Plasma Sheath to Improve the Metal-Dye Electronic Coupling in Dye-Sensitized Solar Cells, Surfaces and Interfaces 23 (2021), https://doi.org/10.1016/j.surfin.2021.101028.
[60] R. Ferwerda, J.H. Van Der Maas, F.B. Van Duijneveldt, Pyridine Adsorption onto Metal Oxides: An Ab Initio Study of Model Systems, J. Mol. Catal. A Chem. 104 (1996) 319–328, https://doi.org/10.1016/1381-1169(95)00179-4.
[61] M.I. Zaki, M.A. Hasan, F.A. Al-Sagheer, L. Pasupulety, In Situ FTIR Spectra of Pyridine Adsorbed on SiO_2-Al_2O_3, TiO_2, ZrO_2 and CeO_2: General Considerations for the Identification of Acid Sites on Surfaces of Finely Divided Metal Oxides, Colloids Surfaces A Physicochem. Eng. Asp. 190 (2001) 261–274, https://doi.org/10.1016/S0927-7757(01)00690-2.
[62] M. Castellà-Ventura, Y. Akacem, E. Kassab, Vibrational Analysis of Pyridine Adsorption on the Brønsted Acid Sites of Zeolites Based on Density Functional Cluster Calculations, J. Phys. Chem. C 112 (2008) 19045–19054, https://doi.org/10.1021/jp8069354.
[63] K.D. Dobson, A.J. McQuillan, In Situ Infrared Spectroscopic Analysis of the Adsorption of Aromatic Carboxylic Acids to TiO_2, ZrO_2, Al_2O_3, and Ta_2O_5 from Aqueous Solutions, Spectrochim. Acta - Part A Mol. Biomol. Spectrosc. 56 (2000) 557–565, https://doi.org/10.1016/S1386-1425(99)00154-7.
[64] M. Buchholz, M. Xu, H. Noei, P. Weidler, A. Nefedov, K. Fink, Y. Wang, C. Wöll, Interaction of Carboxylic Acids with Rutile TiO_2(110): IR-Investigations of Terephthalic and Benzoic Acid Adsorbed on a Single Crystal Substrate, Surf. Sci. 643 (2016) 117–123, https://doi.org/10.1016/j.susc.2015.08.006.
[65] J. Liu, Y. Wang, D. Sun, Enhancing the Performance of Dye-Sensitized Solar Cells by Benzoic Acid Modified TiO_2 Nanorod Electrode, Renew. Energy 38 (2012) 214–218, https://doi.org/10.1016/j.renene.2011.07.028.
[66] J. Singh, A. Gusain, V. Saxena, A.K. Chauhan, P. Veerender, S.P. Koiry, P. Jha, A. Jain, D.K. Aswal, S.K. Gupta, XPS, UV-Vis, FTIR, and EXAFS Studies to Investigate the Binding Mechanism of N719 Dye onto Oxalic Acid Treated TiO_2 and Its Implication on Photovoltaic Properties, J. Phys. Chem. C 117 (2013) 21096–21104, https://doi.org/10.1021/jp4062994.
[67] F. De Angelis, S. Fantacci, E. Mosconi, M.K. Nazeeruddin, M. Grätzel, Absorption spectra and excited state energy levels of the N719 dye on TiO_2 in dye-sensitized solar cell models, J. Phys. Chem. C. 115 (2011) 8825–8831, https://doi.org/10.1021/jp111949a.
[68] K. Awasthi, H.Y. Hsu, E.W.G. Diau, N. Ohta, Enhanced charge transfer character of photoexcited states of dye sensitizer on the N719/TiO_2 interface as revealed by electroabsorption spectra, J. Photochem. Photobiol. A Chem. 288 (2014) 70–75, https://doi.org/10.1016/j.jphotochem.2014.05.001.
[69] Y. Ooyama, Y. Harima, Photophysical and Electrochemical Properties, and Molecular Structures of Organic Dyes for Dye-Sensitized Solar Cells, ChemPhysChem 13 (2012) 4032–4080, https://doi.org/10.1002/cphc.201200218.
[70] X. Guo, Y. Luo, Y. Zhang, X. Huang, D. Li, Q. Meng, X. Guo, Y. Luo, Y. Zhang, X. Huang, Study on the effect of measuring methods on incident photon-to-electron conversion efficiency of dye-sensitized solar cells by home-made setup, Rev. Sci. Instrum. 81 (2010) 103106, https://doi.org/10.1063/1.3488456.
[71] M. Mahbuburrahman, N. Chandradebnath, J.J. Lee, Electrochemical Impedance Spectroscopic Analysis of Sensitization-Based Solar Cells, Isr. J. Chem. 55 (2015) 990–1001, https://doi.org/10.1002/ijch.201500007.
[72] F. Sauvage, A Review on Current Status of Stability and Knowledge on Liquid Electrolyte-Based Dye-Sensitized Solar Cells, Advances in Chemistry 2014 (2014) 939525–939548, https://doi.org/10.1155/2014/939525.
[73] Z. Mao, W. Liu, H. Cai, J. Shi, Z. Wu, Y. Yang, J. Duan, A kinetic/thermodynamic study of transparent co-adsorbents and colored dye molecules in visible light based on microgravimetric quartz-crystal microbalance on porous TiO_2 films for dye-sensitized solar cells, Phys. Chem. Chem. Phys. 22 (2020) 26828–26837, https://doi.org/10.1039/D0CP05403H.
[74] Q. Qu, H. Geng, R. Peng, Q. Cui, X. Gu, F. Li, M. Wang, Chemically Binding Carboxylic Acids onto TiO_2 Nanoparticles with Adjustable Coverage by Solvothermal Strategy, Langmuir 26 (2010) 9539–9546, https://doi.org/10.1021/la100121n.
[75] Y. Harima, T. Fujita, Y. Kano, I. Imae, K. Komaguchi, Y. Ooyama, J. Ohshita, Lewis-Acid Sites of TiO_2 Surface for Adsorption of Organic Dye Having Pyridyl Group as Anchoring Unit, J. Phys. Chem. C 117 (2013) 16364–16370, https://doi.org/10.1021/jp405835y.
[76] N. Martsinovich, D.R. Jones, A. Troisi, Electronic Structure of TiO_2 Surfaces and Effect of Molecular Adsorbates Using Different DFT Implementations, J. Phys. Chem. C 114 (2010) 22659–22670, https://doi.org/10.1021/jp109756g.
[77] I.X. Green, C. Buda, Z. Zhang, M. Neurock, J.T. Yates, IR Spectroscopic Measurement of Diffusion Kinetics of Chemisorbed Pyridine through TiO_2 Particles, J. Phys. Chem. C 114 (2010) 16649–16659, https://doi.org/10.1021/jp1061489.